Geophysical Research Letters

RESEARCH LETTER
10.1029/2020GL091959

Key Points:

- Sea-level trends during 2005–2015 exhibited a meridional asymmetry in the subtropical Pacific Ocean
- This behavior is qualitatively reproduced by a reduced gravity model forced by surface wind stress
- Results suggest an important role for anomalous cross-equatorial Pacific meridional heat flux

Supporting Information:

- Supporting Information S1

Correspondence to:
F. Schloesser,
schloess@hawaii.edu

Citation:
Schloesser, F., Thompson, P. R., & Piecuch, C. G. (2021). Meridional asymmetry in recent decadal sea-level trends in the subtropical Pacific Ocean. *Geophysical Research Letters*, *48*, e2020GL091959. https://doi.org/10.1029/2020GL091959

Received 4 DEC 2020
Accepted 22 FEB 2021

Meridional Asymmetry in Recent Decadal Sea-Level Trends in the Subtropical Pacific Ocean

F. Schloesser[1], P. R. Thompson[1], and C. G. Piecuch[2]

[1]Department of Oceanography, University of Hawai'i at Mānoa, Honolulu, HI, USA, [2]Physical Oceanography Department, Woods Hole Oceanographic Institution, Woods Hole, MA, USA

Abstract Recent sea surface height (SSH) trends in the South Pacific are substantially greater than trends in the North Pacific. Here, we use the Estimating the Climate and Circulation of the Ocean Version 4 Release 4 ocean state estimate and the Ocean Reanalysis System 5 to identify the forcing and mechanisms underlying that meridional asymmetry during 2005–2015. Thermosteric contributions dominate the spatial structure in Pacific SSH trends, but contributions from local surface heat fluxes are small. Wind stress trends drive a spin-up of the South Pacific subtropical gyre and a northward shift of the North Pacific subtropical gyre. A reduced gravity model forced with reanalysis winds qualitatively reproduces the meridional seesaw in sea level, suggesting that asymmetric trends in subtropical wind stress drive a cross-equatorial heat transport. A reversal in forcing associated with this process could impact near-term rates of coastal sea-level change, particularly in Pacific Island communities.

Plain Language Summary Recent sea-surface-height trends in the South Pacific are substantially greater than trends in the North Pacific. Here, we use the Estimating the Climate and Circulation of the Ocean Version 4 Release 4 ocean state estimate and the Ocean Reanalysis System 5 to identify the forcing and mechanisms underlying that meridional asymmetry during 2005–2015. We show that the anomalous sea-level trends are associated with a cross-equatorial transport and Southern Hemisphere accumulation of heat in response to changes in wind forcing.

1. Introduction

Sea-level trends from satellite altimetry (1993–present) show sea level rising faster in the Southern Hemisphere (SH) than in the Northern Hemisphere (NH) (Cabanes et al., 2001; Cazenave & Nerem, 2004; Hamlington et al., 2020; Willis et al., 2004). Consistently, thermosteric sea-level trends from Argo indicate that the SH ocean, which constitutes 57% of the global ocean surface area, accumulated as much as 90% of the heat gained by the global upper ocean (0–2,000 m) since the mid-2000s (Llovel & Terray, 2016; Roemmich et al., 2015). Tide-gauge records suggest the hemispheric asymmetry in sea-level change is a recent phenomenon and unique since at least the middle (and potentially the beginning) of the twentieth century (Merrifield et al., 2009; Thompson & Merrifield, 2014).

Analyses of climate model ensembles show that the forced ocean response to anthroprogenic warming likely contributes to the observed spatial structure in sea-level and warming trends (Fasullo & Nerem, 2018). Disentangling specific or regional-scale features of the forced response from internal climate variability in sea-level observations is challenging, because the patterns associated with forced and internal variability may be neither stationary nor independent (Bindoff et al., 2013; Hamlington et al., 2019). Climate model ensembles indicate that the overall hemispheric imbalance during 2005–2015 (i.e., the period spanned by the Argo studies cited above) is most likely due to a cross-equatorial redistribution of heat associated with internal climate variability rather than the forced response, but the mechanism driving the hemispheric heat transport is unclear (Rathore et al., 2020).

During 2005–2015, the Pacific Ocean substantially contributes to the hemispheric asymmetry in sea-level trends (Figures 2b, S1). A broad region of negative sea-level trend anomalies (i.e., anomalous relative to the global-mean trend) in the subtropical North Pacific is opposed by a similarly broad region of positive sea-level trend anomalies in the subtropical South Pacific. The positive sea-level trends in the South Pacific have been attributed to changes in wind stress in the region, leading to warming of the ocean above 2000 m (Llovel & Terray, 2016) and below 2,000 m (Volkov et al., 2017). The negative trend anomalies in the

subtropical North Pacific are not discussed in the context of hemispheric imbalances in warming, perhaps due to an assumed association with zonal structure in sea level related to canonical modes of North Pacific decadal climate variability (Hamlington et al., 2012; Han et al., 2017; Merrifield et al., 2012). However, when the dominant modes of Indo-Pacific sea-level variability are subtracted from the altimeter observations, the band of negative sea-level trends in the subtropical North Pacific—and the associated hemispheric asymmetry in the Pacific—remains (Hamlington et al., 2019).

Here we focus on the 2005–2015 period discussed above and investigate the dynamical mechanism underlying hemispheric asymmetry in sea-level and upper-ocean warming trends in the Pacific basin. Specifically, we use a reduced gravity model to quantify the impact of changes in wind-driven subtropical gyre circulation on asymmetric sea-level trends.

2. Data and Models

2.1. Data and Model Products

We use the Version 4 Release 4 data-constrained ocean state estimate from the Estimating the Circulation and Climate of the Ocean consortium (ECCOv4r4). The estimate covers the period 1992–2017. This product updates and extends the Release 1 solution described by Forget et al. (2015), which covers 1992–2011. The ocean model resolution is nominally 1° in the horizontal and there are 50 levels in the vertical surface forcing is derived from ERA-Interim. A particularly useful property of ECCOv4r4 is that it is an exact solution to a freely running general circulation model, and observational constraints are imposed in such a way that conservation laws are obeyed and physical consistency is preserved, allowing for meaningful closed budget diagnostics (e.g., Piecuch et al., 2019).

We use Archiving, Validation and Interpretation of Satellite Oceanographic data (AVISO) Level 4 Absolute Dynamic Topography. These multimission altimeter monthly sea-level anomalies are provided on a regular global grid with 0.25° horizontal resolution starting from year 1993.

We use the European Centre for Medium-Range Weather Forecasts (ECMWF) Ocean Reanalysis System 5 (ORAS5) for 1979–2017 (Zuo et al., 2017). The ocean model resolution is 0.25° in the horizontal and there are 75 levels in the vertical. Results presented in this manuscript are based on ensemble member no. 0.

2.2. Reduced Gravity Model

Reduced gravity models (RGMs) have been shown to be useful and able to simulate the first-order, large-scale response to wind forcing in many studies (e.g., Long et al., 2020; Qiu et al., 1997). Here, we consider solutions to equations

$$-fV = -g'Hh_x + \tau^x - \left[\nu U\right], \tag{1}$$

$$fU = -g'Hh_y + \tau^y - \left[\nu V\right], \tag{2}$$

$$h_t + U_x + V_y = 0, \tag{3}$$

where f is the Coriolis parameter; U, V are zonal and meridional transports per unit width; $g' = 0.02$ ms^{-2} is the reduced gravity; $\boldsymbol{\tau} = (\tau^x, \tau^y)$ is the wind stress, and $h(x, y, t)$ is the spatially and temporally varying layer thickness. The constant background layer thickness $H = 330$ m is chosen such that the baroclinic gravity wave speed $c = \sqrt{g'H} \approx 2.5$ ms^{-1}, generally consistent with observations (Chelton & Schlax, 1996). Frictional terms in brackets are retained formally in the limit $\nu \to 0$ s^{-1}, thereby allowing for infinitely narrow western boundary layers to close the circulation. Sea surface height (SSH) η is linearly related to layer depth in the reduced gravity model (RGM),

$$\eta = \frac{\rho_2 - \rho_1}{\rho_2} h + \eta_o, \tag{4}$$

with $\rho_1 = 1025.9$ kg m^{-3} and $\rho_2 = 1028$ kg m^{-3} being the density in the surface and deep layer, respectively, and η_o some constant reference level.

A condition of no flow is imposed on all lateral boundaries of a Pacific Ocean basin extending meridionally from 40°S to 60°N. The eastern (x_e) and western boundary (x_w) is set as in ORAS5. Note that Equations 1–3 assume that adjustments associated with clockwise and counterclockwise propagation of boundary waves in the Southern and NH respectively (e.g., Kawase, 1987; Johnson & Marshall, 2002) occur instantaneously. This assumption is reasonable: For example, the transit time for a boundary wave propagating at gravity wave speed from Sydney to San Diego (propagating first equatorward along the western boundary, then crossing the Pacific at the equator and propagating poleward along the eastern boundary) is a few months, which is fast relative to the decadal timescales of interest here.

Cross differentiation of the inviscid (1) and (2) and substitution into (3) yields

$$f^2 h_t + f\left(-\tau_y^x + \tau_x^y\right) - \beta\left(g' H h_x + \tau^x\right) = 0, \tag{5}$$

which governs the interior ocean solution. Solutions are obtained by integrating westward from the eastern boundary along Rossby wave characteristics, i.e., $h_t = -c_r h_x - w_{ek}$, with $c_r = -\beta c^2 f^{-2}$ being the Rossby wave speed and $w_{ek} = (\tau^y / f)_x - (\tau^x / f)_y$ the Ekman pumping velocity. We tested the impact of altering the Rossby wave speed c_r to match more closely the observed wave speed (Chelton & Schlax, 1996) and found that reasonable alternative selections for the Rossby wave speed did not qualitatively change the outcome or conclusions reported here. In the equatorial region (5°S < y < 5°N), where f is small and Rossby waves cross the Pacific ocean basin within a few months (Chelton & Schlax, 1996), we neglect the h_t-term in Equation 5, thereby obtaining an equilibrium solution at every time step.

At all latitudes, solutions require an eastern boundary condition $h_e = h(x_e, y, t)$ to be determined. Since the boundary wave response is infinitely fast in our model, h_e is directly obtained from the preservation of domain-integrated surface-layer volume in time, $M_o = \int h \, dA$, which follows from continuity and the no-flow boundary condition (In practice, h_e is iterated at every time step such that the solution satisfies mass conservation). We furthermore neglect the effect of alongshore winds, such that (2) implies $h_e(t)$ is constant along the eastern boundary.

The model is forced by ERA-Interim kinematic wind stress, which is also the basis of the boundary conditions for ECCOv4r4 and ORAS5, and RGM solutions are integrated from 1979 to 2017. We also tested the impact of using monthly NCEP/NCAR reanalysis wind stress (years 1948–2016) to confirm the robustness of our results. Initially, h is set to the equilibrium response to the wind stress averaged over the first 15 years. We tested the impact of using different initial conditions (e.g., average over first 5 years), and the impact is negligible for the period of primary interest (2005–2015), presumably because the time of integration before the start of the study period is sufficiently long. Since there is no explicit diffusion in our model, the memory of earlier states is erased primarily as anomalies propagate into the western boundary, where dynamics average over all incoming anomalies.

Meridional heat transports across a latitude are computed from the RGM, and compared to meridional heat transports from ECCOv4r4. Temperature is uniform throughout the RGM surface layer, hence heat transports are proportional to the zonally integrated volume transports in the surface layer, which are (due to the closed boundaries) compensated by opposite transports at depth associated with colder temperatures. Since solutions depend only on density stratification (g') and not directly on temperature, we refrain from defining layer temperatures and scale heat transports such that they have similar amplitudes as those in ECCOv4r4. Specifically, upper-layer volume fluxes are multiplied with a factor 0.45×10^{-7} PW/(m^3/s) to calculate heat fluxes, which with a specific heat of 3994 J/(kg C) and density of 1030 kg/m^3 corresponds to a temperature difference of about 12 °C between layers one and two.

3. Results

3.1. Decadal Averages and Trends

Figure 1a shows the first empirical orthogonal functions (EOFs) of 10 year averages of ECCOv4r4 Pacific sea-level and thermosteric sea-level anomalies, calculated relative to the Pacific Ocean mean, and then averaged over boxes extending 10° in latitude and zonally across the Pacific Ocean basin. Amplitudes are largest, and of opposite sign, in the subtropical/mid-latitude regions in both hemispheres, indicated by gray shading (For brevity, we refer to both of these regions as subtropical in the discussion below, even though the center of gravity occurs at somewhat higher latitudes in the SH.) The corresponding principle components in Figure 1b indicate a swing from anomalously high sea levels in the NH to anomalously low sea levels beginning around 2005, and an opposite swing in the SH (The same pattern is revealed by decadal sea-level anomalies shown in Figure S2.)

These sea-level changes also manifest themselves in trends (Figure 1c) during 2005–2015, which was previously identified as a period of hemispheric imbalance in ocean warming (Rathore et al., 2020). Specifically, trends are positive in the SH and negative in the NH subtropics, with an average amplitude of 2–3 mm yr^{-1}, which is about the same magnitude as the coeval global-mean trend. These trends are consistent among observations (AVISO) and model products (ECCOv4r4 and ORAS5).

The similarity between dynamic and thermosteric sea-level anomalies (Figure 1a and 1b) suggests that these meridionally asymmetric sea-level trends are associated with changes in ocean heat content. The ECCOv4r4 solution provides runtime-averaged horizontal and surface heat fluxes, which allows for offline diagnosis of a closed heat budget (e.g., Piecuch et al., 2019). As expected given the dominance of thermosteric sea-level changes, and consistent with the findings by Rathore et al. (2020), Pacific heat content trends in Figure 1d show a meridional asymmetry similar to that in sea level, with increased accumulation of heat in the SH. Furthermore, the changes in heat content are dominated by the convergence of horizontal heat transports, suggesting meridional redistribution of heat from NH to SH latitudes. The contribution of surface heat fluxes, on the other hand, is generally smaller in magnitude and of opposite sign to the overall heat content trends, thereby suggesting a damping process.

Figure 2 shows global maps for sea-level trends relative to the Pacific mean for ECCOv4r4, AVISO, and ORAS5. The maps indicate that the different products agree well in terms of the large-scale trend patterns. Differences occur on smaller scales associated with mesoscale eddies, which is unsurprising, since mesoscale features are either unresolved or only partially resolved by these models, and so we do not necessarily expect consistency between data and model products on these spatial scales.

3.2. Forcing

Since the meridional asymmetry in sea-level trends is mostly associated with meridional redistribution of heat (Figure 1), wind-forcing is a reasonable candidate for the underlying cause. Figure 3a shows trends in ERA-Interim sea-level pressure and wind stress during 2004–2014. This trend period is chosen assuming a 1-year lag in the sea-level response to wind forcing *via* baroclinic adjustment (This assumption is based on lag-correlation coefficients computed between sea-level anomalies over 10°–30°N from ECCOv4r4, and a steady state version of the RGM driven by annual-mean winds, which peaks at 1-year lag; see Figure S3. Note that large-scale trends in sea-level pressure and wind stress are not strongly sensitive to precise boundaries of that period.) The most coherent change in the Pacific is a strengthening of the South Pacific High, which couples to intensification of SH trade winds and westerlies. A comparatively small reduction in trade-wind strength occurs over the NH latitude range 10°–30°N, which is surprising given the reduction in ocean heat content and negative sea-level trends relative to the Pacific mean.

Figure 3b shows the streamfunction for the mean Sverdrup gyres in the Pacific over the full record length of ERA-Interim (1979–2017; contours) and trends in Sverdrup transport streamfunction (shading) based on ERA-Interim wind-stress trends during 2004–2014. In the SH, the strengthening of the large-scale winds leads to a spin-up of the gyre circulation. In contrast, the NH subtropical gyre weakens south of 30°N and strengthens north of this latitude, indicating a northward shift of the gyre circulation. As the strength and position of the subtropical gyres strongly impact the sea-level topography; these trends in gyre circulation

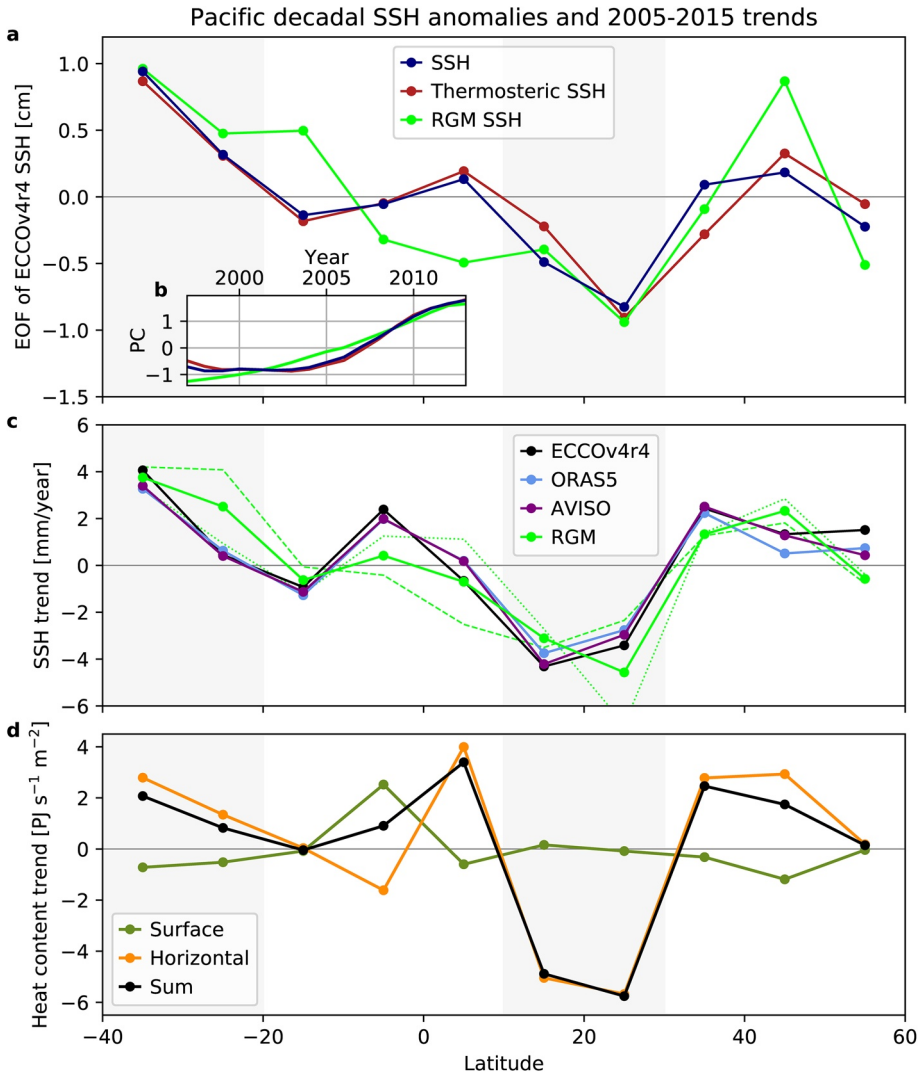

Figure 1. (a) First empirical orthogonal function (EOF) spatial pattern and (b) principle component (PC) time series of 10 year running mean (based on years 1992–2017) Estimating the Climate and Circulation of the Ocean Version 4 Release 4 (ECCOv4r4) Pacific sea surface height (SSH), ECCOv4r4 thermosteric SSH, and Reduced gravity models (RGM) SSH averaged over 10° latitude windows between 40°S and 60°N. (c) Sea-level trends for years 2005–2015 for ECCOv4r4 (black curve), AVISO (purple), ORAS5 (blue), and RGM (green). (d) Heat content trends (black curve), their contributions from horizontal flux convergence (orange curve), surface fluxes (green curve). All anomalies and trends are calculated relative to the Pacific mean. For the RGM, solid curves correspond to the average between solutions with ERA-Interim (dashed curve in panel c) and NCEP winds (dotted curve in panel c).

are generally consistent with the asymmetric sea-level and heat-content trends in Figure 1. Although showing some regional differences, the general trends in wind forcing and Sverdrup transports are similar for NCEP (Figure S4), indicating robustness of the results. Next, we utilize the RGM (Section 2.2) to better quantify their impact.

3.3. Reduced Gravity Model

Figure 3c shows the RGM mean layer thickness associated with the mean Sverdrup circulation (1979–2017), which indicates the characteristic, westward deepening of the thermocline in the subtropical gyres. Layer-thickness trends during 2005–2015 are shown in Figure 3d. The thermocline-depth trends can be translated into sea-level trends using Equation 4, which are compared to those from AVISO, ECCOv4r4, and ORAS5 (Figure 1). The RGM reproduces leading-order features of extra-equatorial structure in the observed

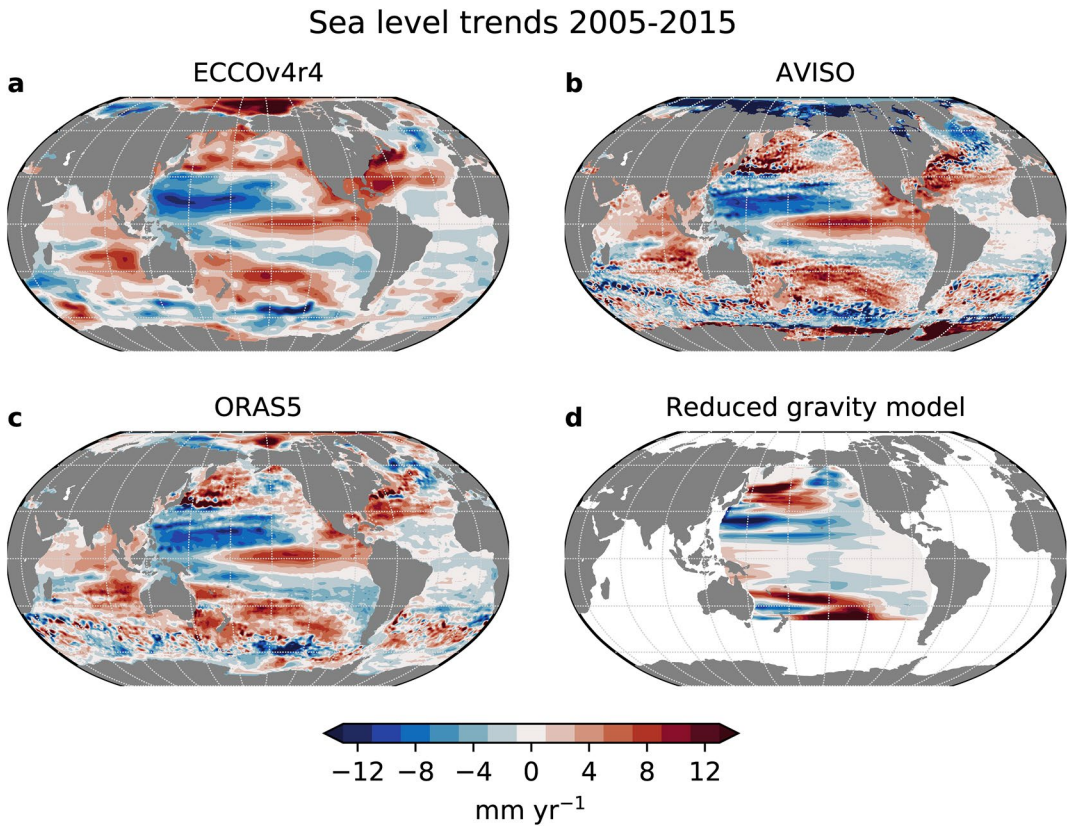

Figure 2. Horizontal maps of sea-level trends over years 2005–2015 for (a) ECCOv4r4, (b) AVISO, (c) ORAS5, and (d) the reduced gravity model (average of solutions with ERA-Interim and NCEP winds). All trends are calculated relative to the Pacific mean.

trends, in particular the hemispheric asymmetry resulting from negative trends in the NH subtropics and strong positive trends in the western parts of the subtropical and midlatitude South Pacific. The meridional asymmetry is reproduced for RGM solutions driven by ERA-Interim as well as NCEP winds (Figure 1c). The greatest differences in spatial structure of the trends from the RGM compared to the observations and reanalysis are along the equator (Figure 2). Due to its simplicity, the RGM is not expected to reproduce observations in the equatorial region due to not resolving equatorial waves, the relatively stronger impact of interannual variability, surface heat fluxes playing a leading role in decadal SSH variability (e.g., Piecuch et al., 2019), and the effect of the Indonesian Throughflow (see Section 3.4). Discrepancies in the equatorial region do not, however, reduce the utility of the RGM for understanding the basic processes leading to hemispheric asymmetry in sea-level trends away from the equator.

Figure 4 compares time series of subtropical North Pacific sea-level anomaly (averaged over $10°N < y < 30°N$) from ECCOv4r4 and RGM (using ERA-Interim winds). Both models show negative trends over the period 2005–2015 (compare Figures 4a and 4b). To isolate the impact of SH winds on these trends, we conducted a RGM sensitivity experiment with the Ekman pumping south of 10°S being replaced by its climatological value. We refer to this sensitivity experiment as RGM-S10. In RGM-S10, the sea-level trend during 2005–2015 in the NH subtropics almost vanishes. This supports the hypothesis that the mechanism most responsible for the asymmetry in sea-level trends during 2005–2015 in the RGM is the wind-driven spin-up of the SH subtropical gyre. As warm surface waters converge into the SH subtropical gyre region and deepen the thermocline there, the basin-wide adjustment (i.e., thinning of the thermocline elsewhere) occurs via boundary waves propagating equatorward along the western boundary, then eastward across the basin at the equator, and finally poleward along the eastern boundary. In the absence of strong surface forcing over subtropical latitudes of the NH, Rossby waves radiate into the basin from the eastern boundary, shoaling the thermocline and reducing sea level (Fu & Qiu, 2002) (note that our model does not explicitly resolve

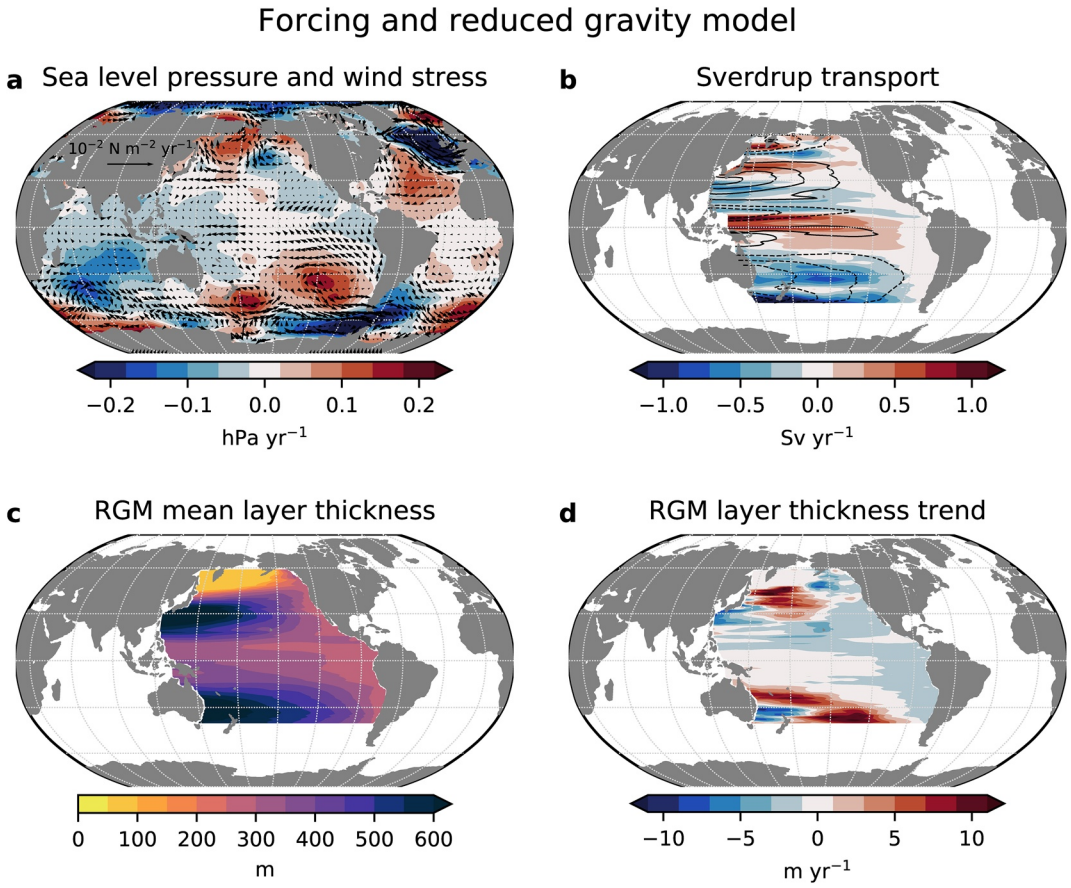

Figure 3. Horizontal maps (a) 2004–2014 trends of ERA-Interim sea-level pressure (shading) and wind stress (arrows), (b) trends in Sverdrup transport in the Pacific (shading) and stream function of the mean circulation (contour interval 10 Sv), (c) Mean layer thickness in the RGM with ERA-Interim winds, and (d) RGM layer thickness trends over years 2005–2015.

boundary waves, and these implicit boundary adjustments occur instantaneously, Section 2.2). A similar pattern occurs with NCEP winds (Figures S4 and S5), however, with the relative impact of NH winds on the NH sea-level trends being larger. To further test the hypothesis that changes in gyre circulation drive a hemispheric redistribution of upper-ocean waters, we analyze Pacific meridional heat fluxes.

3.4. Meridional Heat Fluxes

Figure 4b and 4c show ECCOv4r4 Pacific annual mean meridional heat flux anomalies (i.e., with the time-mean removed) across 10°N and 10°S. While both time series exhibit strong interannual variability, they reveal a tendency for fluxes to be negative relative to their time means (i.e., anomalous redistribution of heat from north to south) during the period 2005–2015. These tendencies are emphasized in the 9 year running means shown in Figure 4d, and are consistent with our previous results as well as those of Rathore et al. (2020). In agreement with the earlier analysis, the RGM captures the decadal trends, and some of the interannual variability (Figure 4b and 4c; 9 year running means are shown in Figure S6; see Section 2.2 for how meridional heat fluxes are calculated in the RGM).

The assumption of closed boundaries in the RGM implies that heat is redistributed within the Pacific on the decadal timescales, which may not hold strictly in reality, since the Pacific Ocean is not a closed basin. The goodness of the closed-boundary assumption used in the RGM is tested by calculating ECCOv4r4 heat fluxes across the RGM domain boundaries (Figure 4d). The flux across 60°N and 40°S are at least an order of magnitude smaller than those across 10°S and 10°N, suggesting that the assumption is reasonable, and

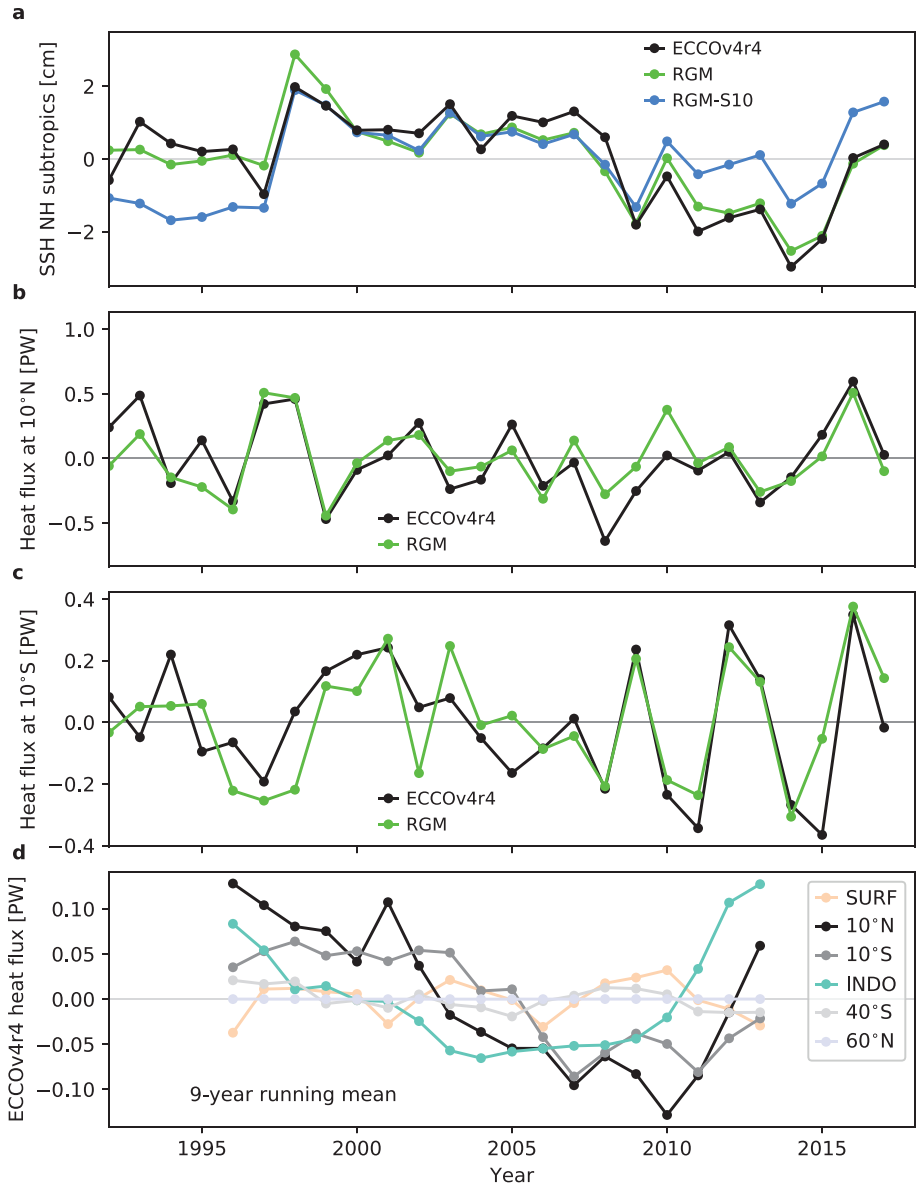

Figure 4. (a) Time series of SSH averaged in the Northern Hemisphere subtropical Pacific, 10°N < y < 30°N, for ECCOv4r4 (black curve), the reduced gravity model with ERA-Interim winds (RGM, green curve), and the RGM with climatologic forcing south of 10°S (RGM-S10, blue curve). The Pacific annual mean meridional heat fluxes across (b) 10°N and (c) 10°S in ECCOv4r4, and the RGM. Panel (d) shows 9 year running means of meridional ECCOv4r4 anomalous heat fluxes in the Pacific across latitude sections at 40°S (light gray curve), 10°S (dark gray curve), 10°N (black curve), and 60°N (lavender curve). Also shown is the heat flux anomaly through the Indonesian Throughflow (turquoise curve; positive means into the Pacific) and the surface heat flux anomaly between 10°S and 10°N (orange curve).

hemispheric exchange of heat between the subtropical basins in the Pacific is much larger than exchange with other ocean basins on decadal timescales.

Anomalies of Indonesian Throughflow heat fluxes (calculated as the sum of the fluxes through the four open sections between Malaysia, Sumatra, Java, Lombok, and Australia), on the other hand, are of similar magnitudes and—on decadal scales—correlate well with the discrepancy between heat fluxes at 10°S and 10°N. This is consistent with previous findings (Mayer et al., 2018) that the Indonesian Throughflow has important implications for the equatorial Pacific heat content. However, basic physical considerations, namely the symmetric poleward propagation of eastern boundary Kelvin waves (e.g., Kawase, 1987; Johnson &

Marshall, 2002) suggest that fluxes through the Indonesian Throughflow do not substantially impact the Pacific sea-level trend difference between NH and SH subtropics of primary interest here.

4. Summary

We have assessed the impact of changes in wind-driven gyre circulation on sea-level trends and redistribution of heat in the Pacific over the period 2005–2015. Our results suggest that this mechanism substantially contributes to previously identified meridionally asymmetric trends in sea level and heat content (Rathore et al., 2020). Specifically, an intensification of the South Pacific High leads to a strengthening of SH winds, and a spin up of the subtropical gyre. In the NH, the subtropical gyre shifts northward, but does not show an increase in strength. This difference leads to a deepening of the SH thermocline relative to the NH, which is associated with an anomalous, interhemispheric heat transport and thermosteric sea-level trend in the SH subtropics at the expense of NH heat content. On the large scale, the sea-level trends associated with this seesaw pattern are of the order of several mm/year, which is comparable to the magnitude of recent global-mean sea-level trends (Beckley et al., 2017; Church & White, 2006).

Finally, while our analysis indicates a coherent shift in the meridional structure of Pacific sea-level trends, dominated by changes in the subtropics, the results do not necessarily suggest that hemispheric asymmetry is the result of an internal ocean or climate mode. The results do, however, provide a mechanism whereby interhemsipheric heat exchange and hemispheric asymmetry in sea-level trends relate to subtropical wind forcing that could result from forced or unforced climate variability. Ultimately, the satellite-altimetry record may be too short to unambiguously distinguish decadal and longer period variability from forced secular trends, and the trends identified here could result from integration of shorter scale variability. Since the Rossby wave speed decreases with latitude, zonal thermocline slopes and depth anomalies tend to increase (Equation 5), and so does the potential for larger sea-level trends (relative to the basin mean) on decadal and longer timescales. In other words, while the ocean generally integrates and acts as a low-pass filter for atmospheric forcing (Hasselmann, 1976), the timescales of the ocean response increase with latitude. This view is consistent with our finding of subtropical dynamics to be increasingly important on decadal timescales, whereas the interhemispheric transport has been shown to be dominated by tropical processes on shorter time scales (McGregor et al., 2014).

Data Availability Statement

ECCOv4r4 data are available at https://ecco.jpl.nasa.gov, ORAS5/ERA-Interim at https://icdc.cen.uni-hamburg.de, NCEP/NCAR fields at http://cmip5.whoi.edu and AVISO at https://www.aviso.altimetry.fr.

Acknowledgments
F. Schloesser and P. R. Thompson were supported by NASA grant 80NSSC17K0564 and NSF grant 1558980. C. G. Piecuch was supported by the NASA Sea Level Change Team (grant 80NSSC20K1241). The authors thank the anonymous reviewer for their helpful comments.

References

Beckley, B. D., Callahan, P. S., Hancock, D., Mitchum, G., & Ray, R. (2017). On the "cal-mode" correction to topex satellite altimetry and its effect on the global mean sea level time series. *Journal of Geophysical Research: Oceans*, *122*(11), 8371–8384. https://doi.org/10.1002/2017JC013090

Bindoff, N. L., Stott, P. A., AchutaRao, K. M., Allen, M. R., Gillett, N., Gutzler, D., et al. (2013). Detection and attribution of climate change: From global to regional. In *Climate change 2013: The physical science basis. Contribution of working group I to the fifth assessment report of the intergovernmental panel on climate change*, Cambridge, UK: Cambridge University Press.

Cabanes, C., Cazenave, A., & Le Provost, C. (2001). Sea level change from Topex-Poseidon altimetry for 1993–1999 and possible warming of the Southern Oceans. *Geophysical Research Letters*, *28*(1), 9–12. https://doi.org/10.1029/2000GL011962

Cazenave, A., & Nerem, R. S. (2004). Present-day sea level change: Observations and causes. *Reviews of Geophysics*, *42*, RG3001. https://doi.org/10.1029/2003RG000139

Chelton, D. B., & Schlax, M. G. (1996). Global observations of oceanic Rossby waves. *Science*, *272*(5259), 234–238.

Church, J. A., & White, N. J. (2006). A 20th century acceleration in global sea-level rise. *Geophysical Research Letters*, *33*, L01602. https://doi.org/10.1029/2005GL024826

Fasullo, J. T., & Nerem, R. S. (2018). Altimeter-era emergence of the patterns of forced sea-level rise in climate models and implications for the future. *Proceedings of the National Academy of Sciences*, *115*(51), 12944–12949. https://doi.org/10.1073/pnas.1813233115

Forget, G., Campin, J., Heimbach, P., Hill, C., Ponte, R., & Wunsch, C. (2015). ECCO version 4: An integrated framework for non-linear inverse modeling and global ocean state estimation. *Geoscientific Model Development*, *8*(10), 3071–3104.

Fu, L.-L., & Qiu, B. (2002). Low-frequency variability of the north Pacific Ocean: The roles of boundary-and wind-driven baroclinic rossby waves. *Journal of Geophysical Research: Oceans*, *107*(C12), 3220. https://doi.org/10.1029/2001JC001131

Hamlington, B. D., Fasullo, J. T., Nerem, R. S., Kim, K., & Landerer, F. W. (2019). Uncovering the pattern of forced sea level rise in the satellite altimeter record. *Geophysical Research Letters*, *46*, 4844–4853. https://doi.org/10.1029/2018GL081386

Hamlington, B. D., Gardner, A. S., Ivins, E., Lenaerts, J. T. M., Reager, J. T., Trossman, D. S., et al. (2020). Understanding of contemporary regional sea-level change and the implications for the future. *Reviews of Geophysics*, *58*(3). e2019RG000672. https://doi.org/10.1029/2019RG000672

Hamlington, B. D., Leben, R. R., Wright, L. A., & Kim, K. Y. (2012). Regional sea level reconstruction in the Pacific Ocean. *Marine Geodesy*, *35*(suppl. 1), 98–117. https://doi.org/10.1080/01490419.2012.718210

Han, W., Meehl, G. A., Stammer, D., Hu, A., Hamlington, B., Kenigson, J., et al. (2017). Spatial Patterns of sea level variability associated with natural internal climate modes. *Surveys in Geophysics*, *38*(1), 217–250. https://doi.org/10.1007/s10712-016-9386-y

Hasselmann, K. (1976). Stochastic climate models part i. theory. *Tellus*, *28*(6), 473–485.

Johnson, H. L., & Marshall, D. P. (2002). A theory for the surface Atlantic response to thermohaline variability. *Journal of Physical Oceanography*, *32*, 1121–1132.

Kawase, M. (1987). Establishing of deep ocean circulation driven by deep-water production. *Journal of Physical Oceanography*, *17*, 2294–2317.

Llovel, W., & Terray, L. (2016). Observed southern upper-ocean warming over 2005–2014 and associated mechanisms. *Environmental Research Letters*, *11*(12), 124023. https://doi.org/10.1088/1748-9326/11/12/124023

Long, X., Widlansky, M. J., Schloesser, F., Thompson, P. R., Annamalai, H., Merrifield, M. A., & Yoon, H. (2020). Higher sea levels at Hawaii caused by strong El Niño and weak trade winds. *Journal of Climate*, *33*(8), 3037–3059.

Mayer, M., Alonso Balmaseda, M., & Haimberger, L. (2018). Unprecedented 2015/2016 Indo-Pacific heat transfer speeds up tropical Pacific heat recharge. *Geophysical Research Letters*, *45*, 3274–3284. https://doi.org/10.1002/2018GL077106

McGregor, S., Spence, P., Schwarzkopf, F. U., England, M. H., Santoso, A., Kessler, W. S., et al. (2014). ENSO-driven interhemispheric Pacific mass transports. *Journal of Geophysical Research: Oceans*, *119*(9), 6221–6237. https://doi.org/10.1002/2014JC010286

Merrifield, M. A., Merrifield, S. T., & Mitchum, G. T. (2009). An anomalous recent acceleration of global sea level rise. *Journal of Climate*, *22*(21), 5772–5781. https://doi.org/10.1175/2009JCLI2985.1

Merrifield, M. A., Thompson, P. R., & Lander, M. (2012). Multidecadal sea level anomalies and trends in the western tropical Pacific. *Geophysical Research Letters*, *39*, 2–6. https://doi.org/10.1029/2012GL052032

Piecuch, C. G., Thompson, P. R., Ponte, R. M., Merrifield, M. A., & Hamlington, B. D. (2019). What caused recent shifts in tropical Pacific Decadal sea-level trends?. *Journal of Geophysical Research: Oceans*, *124*, 7575–7590. https://doi.org/10.1029/2019JC015339

Qiu, B., Miao, W., & Müller, P. (1997). Propagation and decay of forced and free baroclinic Rossby waves in off-equatorial oceans. *Journal of Physical Oceanography*, *27*(11), 2405–2417.

Rathore, S., Bindoff, N. L., Phillips, H. E., & Feng, M. (2020). Recent hemispheric asymmetry in global ocean warming induced by climate change and internal variability. *Nature Communications*, *11*(1), 1–8. https://doi.org/10.1038/s41467-020-15754-3

Roemmich, D., Church, J., Gilson, J., Monselesan, D., Sutton, P., & Wijffels, S. (2015). Unabated planetary warming and its ocean structure since 2006. *Nature Climate Change*, *5*(3), 240–245. https://doi.org/10.1038/nclimate2513

Thompson, P. R., & Merrifield, M. A. (2014). A unique asymmetry in the pattern of recent sea level change. *Geophysical Research Letters*, *41*, 1–9. https://doi.org/10.1002/2014GL061263

Volkov, D. L., Lee, S.K., Landerer, F. W., & Lumpkin, R. (2017). Decade-long deep-ocean warming detected in the subtropical South Pacific. *Geophysical Research Letters*, *44*, 927–936. https://doi.org/10.1002/2016GL071661

Willis, J. K., Roemmich, D., & Cornuelle, B. D. (2004). Interannual variability in upper ocean heat content, temperature, and thermosteric expansion on global scales. *Journal of Geophysical Research*, *109*, 1–13. https://doi.org/10.1029/2003JC002260

Zuo, H., Balmaseda, M. A., & Mogensen, K. (2017). The new eddy-permitting ORAP5 ocean reanalysis: Description, evaluation and uncertainties in climate signals. *Climate Dynamics*, *49*(3), 791–811.